



Spectrum splitting through CuS–ZnO/water hybrid nanofluid for agricultural greenhouse cooling applications: An experimental study

Muhammad Usman Sajid¹ · M. Ziad Saghir² · Ibrahim Dincer³ · Yusuf Bicer¹

Received: 17 October 2022 / Accepted: 15 December 2022 / Published online: 16 January 2023
© The Author(s) 2023

Abstract

In the present work, CuS–ZnO/water hybrid nanofluids (in concentrations of 0.0025 mass% and 0.005 mass%) are synthesized using a two-step method with nanoparticles composition of 95% CuS and 5% ZnO. The optically tuned nanofluid filter on the agricultural greenhouse roof can reduce the cooling load by transmitting the visible spectrum and absorbing the near-infrared radiation in the solar spectrum. The size distribution of nanoparticles, stability and optical transmission of both concentrations in the visible and near-infrared regions are examined. Two hollow containers (i.e., ducts) with thicknesses of 4 mm and 8 mm are prepared. Each of these ducts is attached to a greenhouse unit and placed in front of a solar simulator. The experimental results reveal that applying CuS–ZnO nanofluid reduces the inside temperature of the greenhouse unit under all irradiance and ambient temperature ranges. The cooling system gains an average of 27.4% less heat from the greenhouse unit when the CuS–ZnO nanofluid flows through an 8 mm duct compared to no-fluid case (empty duct). The photothermal conversion efficiency of nanofluid is found to be higher than the one for water. The crop growth factor of 82.2% is obtained for 8 mm duct case, and the photosynthetic photon flux density inside the greenhouse unit is reduced without affecting the growth of many plants. Furthermore, the payback period of the nanofluid system (with 8 mm duct) is calculated as 0.42 years, and the application of optically tuned nanofluid can help reduce the cooling system's size and energy requirement for cooling.

Keywords Cooling load · Thermal management · Efficiency · Nanofluids · Radiation · Calorimetry

List of symbols

A	Area, m ²	$I_o(\lambda)$	Incident radiant flux, W m ⁻² nm ⁻¹
C_C	Initial capital cost, \$	I	Solar radiation intensity, W m ⁻²
C_E	Cost of electricity, \$ kWh ⁻¹	i_R	Interest rate, %
$C_{O\&M}$	Annual operating and maintenance cost, \$ m ⁻²	L_p	Life period, years
C_p	Specific heat, kJ kg ⁻¹ °C ⁻¹	\dot{m}	Mass flow rate, kg s ⁻¹
C_{SE}	Annual cost saving in electricity, \$ m ⁻²	m	Mass, kg
E_S	Electrical energy saved, kWh m ⁻²	T	Temperature, °C
f_R	Inflation rate, %	x	Greenhouse cover thickness, mm
G	Crop growth factor, %	P_{BP}	Payback period, years
		$\dot{Q}_{cooling}$	Heat gained, kJ
		Z	Best estimate of variable

✉ Muhammad Usman Sajid
musajid@hbku.edu.qa

¹ Division of Sustainable Development, College of Science and Engineering, Hamad Bin Khalifa University, Qatar Foundation, Doha, Qatar

² Department of Mechanical and Industrial Engineering, Toronto Metropolitan University, Toronto, Canada

³ Clean Energy Research Laboratory, Faculty of Engineering and Applied Science, Ontario Tech. University, 2000 Simcoe Street North, Oshawa, ON L1G 0C5, Canada

Greek symbols

α	Absorption spectrum, %
ρ	Density, kg m ⁻³
η	Efficiency, %
τ	Transmittance, %
\varnothing	Volume fraction, %
λ	Wavelength, nm

Subscripts

bf	Base fluid
in	Inlet
nf	Nanofluid
np	Nanoparticle
out	Outlet
th	Thermal

Abbreviations

CuS	Copper mono sulfide
PAR	Photosynthetically active radiations
PPFD	Photosynthetic photon flux density
ST-OSC	Semi-transparent organic solar cells
ST-PSC	Semi-transparent polymer solar cells
ZnO	Zinc oxide

Introduction

The solar spectrum is usually categorized into three regions: Ultraviolet, visible, and infrared. The solar radiations having a wavelength less than 400 nm are in the ultraviolet region, and the radiations with wavelengths ranging between 400 and 800 nm are in the visible region. Radiations with a wavelength greater than 800 nm are classified as infrared radiations. Plants mainly utilize the visible spectrum in the sunlight during photosynthesis to prepare their food. Numerous factors can negatively affect the food security of a country/region; climate change is one of them, as it can reduce crop production in open fields or protected environments. The areas with extremely high ambient temperatures and solar irradiance do not favor the cultivation of crops in open fields. Agricultural greenhouses proved to be an efficient way to produce crops in harsh weather conditions with the help of distinct cooling units. Infrared radiation, also known as heat radiation, enters the greenhouse and causes a rise in the temperature. Suppose the temperature inside the greenhouse is higher than the optimum temperature of the crop. In that case, it can negatively affect crop productivity and increase irrigation water use, which is one of the challenges

in regions with water scarcity. The plants may die if exposed to a higher temperature for longer periods.

The higher temperatures inside greenhouses will require a cooling system to remove the accumulated heat. The infrared radiations are a primary source of this heat accumulation inside the greenhouse. The blockage of these radiations could help to reduce the temperature of the greenhouse. This consistent decline in temperature will lead to a reduction in sizing and the energy requirement of the cooling system. The majority of cooling systems require electricity to operate, and most of the electricity is produced through the burning of fossil fuels, which results in emissions. Thus, reducing electricity consumption by the cooling system will help to reduce emissions and make the system more efficient and environmentally friendly. As an alternative solution, here, we apply a spectrum-selective nanofluid as a filter to reduce this heat accumulation inside the greenhouse. Several researchers have already used various methods to adjust or use the solar spectrum for greenhouse applications, as shown in Fig. 1.

The ST-OSC provide an opportunity to produce eco-friendly off-grid power for agriculture greenhouses activities. The walls/roof of the greenhouse could be made of these ST-OSC, which are spectrally engineered to transmit the visible spectrum of sunlight. The ST-OSC (prepared from non-halogenated solvents) installed on the rooftop of the greenhouse displayed a power conversion efficiency of 13.08% with a crop growth factor of 24.7% [1]. Though the power conversion efficiency of ST-OSC is reasonable, the crop growth factor is questionable as its value is low, which indicates that the ST-OSC use a significant portion of the visible spectrum in the power conversion process. Ravishankar et al. [2] investigated the impact of ST-OSC on lettuce growth using three various ST-OSC films. The maximum power conversion efficiency of ST-OSC film was about 5.19%, with an average of 38% transmission in photosynthetically active radiations (PAR). The open literature shows that the power conversion efficiency of ST-OSC is usually less than 10%, with average visible transmittance of less than 50% [3]. The power conversion efficiency can be

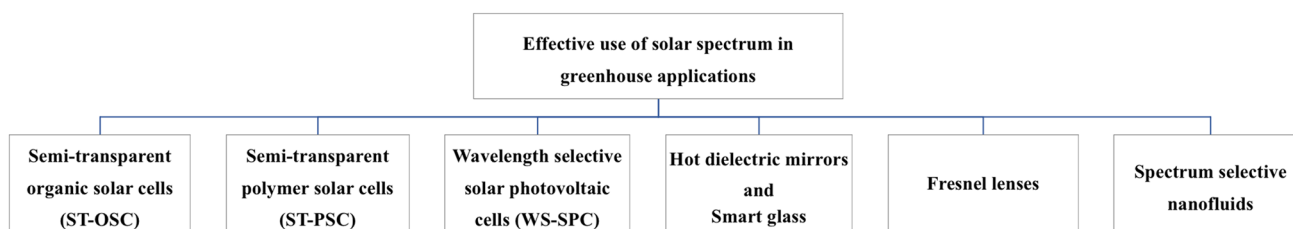


Fig. 1 Classification of several methods using solar spectrum in greenhouse applications

enhanced at the cost of visible spectrum transmission. The ST-OSC developed in the study [4] have a power conversion efficiency of 13.15%, with an average visible transmittance of 25.9%.

The flexible ST-OSC are prepared in the study [5] for greenhouse applications to avoid the mechanical brittleness of electrodes. The flexible ST-OSC can achieve a power conversion efficiency of 10% with 21% transmittance in the visible spectrum of sunlight. The semi-transparent polymer solar cells (ST-PSC) could be another option for greenhouse applications. The power conversion efficiency of ST-PSC reached to 7.7%, with a defined crop growth factor of 24.8% [6]. Hu et al. [7] fabricated ST-PSC with PM6:Y6 as active layers. The ST-PSC has a good power conversion efficiency of 12.37%, with a poor average visible transmittance of 18.6%. Wavelength-selective solar photovoltaics (WS-SPV) have the potential to absorb a specified portion of the solar spectrum for electricity generation and transmit the remaining for the photosynthesis of plants. Loik et al. [8] used WS-SPV as the greenhouse walls and roof. The WS-SPV were produced from the embedment of luminescent solar concentrators and conventional silicon PVs into the polymethyl methacrylate. Their WS-SPV attained a theoretical power conversion efficiency of 9.4% with high PAR absorption (about 64%).

Bicer et al. [9] proposed a novel greenhouse roof concept incorporating dielectric mirrors (hot mirrors) and solar photovoltaic modules working under infrared radiations. The sun-tracking roof splits the solar spectrum through dielectric mirrors. The dielectric mirrors transmit the visible spectrum to the plants inside the greenhouse and simultaneously reflect the infrared radiations to the vertically aligned solar photovoltaics (having an active window in the infrared region). Their technique helps to meet the electricity requirement of greenhouses located in hot arid climates partially or completely. The capital costs of components used in this study are still high, which is the main hindrance to this idea's practical application. The smart glass film ULR-80 with specialized optical characteristics (which blocked 19% of red light and 58% of the far-red) was applied to an agricultural greenhouse containing eggplants [10]. The blockage of far-red radiations resulted in 8% heat load reduction, which reduced water consumption by 18%. The smart glass film was blocking some portion of red light that takes part in photosynthesis, resulting in a 28% reduction of total seasonal fruit.

Pakari and Ghani [11] installed the negative Fresnel lenses on the roof of a thermally insulated greenhouse. The lens arrangement ensured that the solar irradiance was distributed on the rows of plants. The proposed method could provide the solar irradiance necessary for tomato plant growth. This technique helped to reduce the greenhouse cooling load by 80%. Sonneveld et al. [12] proposed a new design that combines the hybrid photovoltaic/thermal (PVT) system with the near-infrared reflective film and is installed

on a greenhouse's roof. When the solar spectrum incident on this reflective film, the visible spectrum will pass through it, and the infrared radiations will be reflected to the PVT system. Their system provided 18.2 kWh m⁻² of electrical energy per annum. Alinejad et al. [13] investigated the environmental and economic aspects of a solar photovoltaic blind system installed on the roof of a rose greenhouse. Their analysis covered 14 different configurations of these photovoltaics on the roof. The photovoltaics can produce about 42.7 kWh m⁻² of electrical energy annually by covering 19.2% area of the greenhouse roof.

The nanofluids, which contain nanosized particles in the water or other base fluids, are being used by many researchers to enhance the heat transfer of shell and helical coil heat exchangers [14], heat sinks [15], and automobile radiators [16], etc. The optical transmittance of water in the visible region of solar spectrum is high (nearly 90% for an optical path length of 10 mm), while it has the potential to block a significant portion of infrared radiations [17]. These optical characteristics of water made them a natural potential candidate for greenhouse application where visible spectrum transmission is required. Further addition of a small quantity of nanosized particles in water (results in nanofluid) can significantly change its optical transmission characteristics [18]. These nanofluids have the potential to block a specified portion of solar spectrum and transmit other. This characteristic of nanofluids made them a prominent candidate for spectrum-splitting applications. The application of Ag@SiO₂/propylene glycol nanofluid [19] and Ag@TiO₂ nanofluid [20] as beam splitters in the PVT system enhanced the thermal efficiency and merit function. The spectrum-splitting applications of nanofluids can be found in parabolic trough solar collectors [21], evacuated tube collectors [22], flat plate solar collectors [23], solar desalination system [24], and solar dish collectors [25].

A few studies recently investigated the potential of spectrum-selective nanofluids for greenhouse and building applications. Yuan et al. [26] synthesized the ATO-WO₃/water nanofluids, which have high transmittance (about 79.56% for an optical path of 10 mm) in the visible region and can absorb (about 66%) the infrared radiations. The results showed that the nanofluids could attain a photothermal conversion efficiency of 34.4% with a crop growth factor of 93.6%. Liu et al. [27] used ATO/water nanofluid for buildings in tubular daylighting devices. The results showed a saving of 30.9 kWh of electricity for refrigeration. Sajid and Bicer [28] thermodynamically assessed the performance of an integrated system that incorporates a spectrum-selective roof with nanofluid, desalination unit, vapor absorption cooling system, and greenhouse. The spectrum-selective nanofluid flows through the greenhouse roof to block the infrared radiations. The analysis revealed that the circulation of nanofluid through greenhouse roof could reduce

the cooling load by 26%. The major drawbacks associated with various techniques (ST-OSC, ST-PSC, WS-SPV, smart glass, Fresnel lenses, and dielectric mirrors) used for spectrum splitting or full solar spectrum utilization for greenhouse applications can be summarized as follows:

- The transmittance of ST-OSC, ST-PSC, smart glass, Fresnel lenses, dielectric mirrors, and WS-SPVs is fixed and cannot be changed according to season. So, the plants may face excessive shading during winter, reducing crop productivity.
- The transmittance of these solar cells (ST-OSC, ST-PSC, and WS-SPV) is very low in the photosynthetically active region, which can affect plant growth negatively. For most crops, 1% reduction in photosynthesis can reduce crop production by 1% [29].
- Solar cells utilize the infrared spectrum for power generation, but their power conversion efficiencies are very low.
- The capital cost of some methods (e.g., [9]) is too high.

Note that spectrum-selective nanofluids can provide unique solutions to the aforementioned problems efficiently and sustainably. The proposed method in this work has the potential to overcome these problems without making any significant changes in the structural design of agricultural greenhouses in a more cost-effective manner. The transmittance in the visible spectrum can be controlled by changing the concentration of nanofluids. So, the concentration of nanofluids can be adjusted accordingly (depending on the season) to maintain the required transmission of PAR inside the greenhouse. Nanofluid will absorb the infrared radiations, which do not take part in photosynthesis. The temperature of nanofluids will rise after absorbing these infrared radiations in the solar spectrum. This higher-temperature nanofluid can be used as an energy input for many applications. In this way, the application of spectrum-selective nanofluids will allow full solar spectrum utilization. The application of spectrum-selective nanofluids for agricultural greenhouses is still at an immature level of understanding and still requires an extensive amount of work in this specific field. Hence, this study experimentally investigates the potential of spectrum-selective CuS–ZnO/water hybrid nanofluid for greenhouse applications under various ambient conditions and the thickness of nanofluid layer (duct thickness of 4 mm and 8 mm). The optically tuned CuS–ZnO/water nanofluid has high transmittance in the visible region of solar spectrum, with the potential to block the unwanted infrared radiations (that do not take part in the photosynthesis). The specific objectives of the present experimental investigation are sixfold, as stated below:

- To prepare optically tuned CuS–ZnO/water nanofluids (having concentrations of 0.0025 mass% and

0.005 mass%) and investigate the stability and nanoparticle size distribution of the currently prepared nanofluids.

- To examine the optical transmission of prepared concentrations of CuS–ZnO/water nanofluids and calculate the plant growth factor based on the transmittance of nanofluids.
- To prepare an experimental greenhouse setup by fabricating the ducts with various depths (4 mm and 8 mm) through which the water and nanofluid flow and then evaluate the cooling load reduction potential of nanofluids under different ambient temperatures conditions.
- To investigate the impacts on heat gained by the cooling system and on inside temperature of greenhouse unit with and without nanofluid applications.
- To assess the nanofluid flow rate and duct thickness effect on the photothermal conversion efficiency.
- To study the economic feasibility of applying CuS–ZnO/water nanofluid in agricultural greenhouses in hot regions with cooling requirements.

Materials and methods

Preparation of nanofluids

The ZnO nanopowder (having particles size between 35 and 45 nm, and density 5606 kg m^{-3}) and CuS powder (particles size < 100 mesh, and density 4760 kg m^{-3}) are acquired from US-nano and Sigma-Aldrich, respectively. The deionized water is used as base fluid due to higher transmission in PAR and strong absorption in the near-infrared region (a requirement for agricultural greenhouse). The wet ball milling (Retsch, Emax, Germany) method is employed to reduce the size of CuS particles for better suspension in the base fluid. The specific amount (0.95 g) of CuS powder is weighted (using weight balance EX225D, OHAUS, USA) and mixed with the same quantity of (Cetyltrimethylammonium bromide (CTAB)) surfactant. After adding 10 mL of water, this mixture is subjected to ball milling operation for 13 h (at 800 rpm). The ball-to-material ratio used in the ball milling operation is 10:1. The ball milling equipment is programmed to take a pause for 5 min after 15 min of operation. To avoid high temperatures during ball milling operation, the temperature range of procedure is set as 25–40 °C. After cleaning the balls and jars of ball milling equipment using deionized water, 0.05 g of ZnO nanopowder is added to this mixture. For homogenous suspension of CuS–ZnO particles, this mixture is subjected to ultrasonication (Qsonica, Q500, USA) for 30 min. The CuS–ZnO/water nanofluid has a composition of 95% CuS and 5% ZnO particles. The optically tuned nanofluids are prepared for greenhouse application. That is why the concentration selection of nanofluid is mainly dependent on optical transmittance.

Based on the optical transmittance, two mass concentrations, 0.0025 mass% and 0.005 mass%, are selected for experimental work by diluting the concentrated solution. The low concentration (0.0025 mass%) is prepared for a duct with a higher thickness (8 mm), while the high concentration (0.005 mass%) is for a duct with low thickness (4 mm). The ball equipment, probe-sonicator, and prepared nanofluid samples are depicted in Fig. 2.

Stability and particle size distribution

The nanofluids perform effectively if the nanoparticles remain suspended in the base fluid uniformly and homogeneously. If the nanoparticles start to agglomerate, particles will be settled. This settlement of nanoparticles reduces the performance of the applied system. The nanoparticles suspended in the base fluid could have either attractive or repulsive forces. If the attractive forces surpass the repulsive forces, the particles tend to agglomerate. In contrast, if repulsive forces dominate the attractive forces, the particles may remain suspended for longer durations [30]. The zeta potential method is commonly used to investigate the stability of nanofluids. The zeta potential method provides information about the charge developed at the interface of nanoparticle and its liquid (water) medium. Zetasizer Nano (ZSP (ZEN5600), UK) is used to examine the stability of nanofluid in this study. The nanofluids having zeta potential values between ± 30 –45 mV are considered physically stable [31]. The folded capillary cell (DTS1070) is used during the

zeta potential analysis. Figure 3a and c illustrates the zeta potential values of low concentrated (0.0025 mass%) and high concentrated (0.005 mass%) CuS–ZnO/water nanofluid, respectively. The zeta potential values of prepared nanofluids are close to 45 mV, which means the nanofluids are stable. No sedimentation is observed in visual inspection even after experiments (after 100 days of nanofluid preparation), which confirms that the nanofluids are stable.

The graphs in Fig. 3b and d represent the nanoparticle size distribution in the base fluid for low and high concentrated nanofluids, respectively. The suspended particle size is small for low concentrated nanofluid than the high concentrated nanofluid. The possible reason for this phenomenon is that higher concentrated nanofluid has more numbers of nanoparticles. The large number of nanoparticles has a higher tendency to aggregate in the fluid than the low quantity of nanoparticles. Figure 3b and d confirms this phenomenon. The instrument Zetasizer Nano (ZSP (ZEN5600), UK) is able to measure the size of particles in the range of 0.3 nm–10 μm by utilizing the dynamic light scattering (DLS) method. It is also evident from Fig. 3b and d that the ball milling process effectively reduced the size of CuS particles.

Optical properties

For agricultural greenhouses, the transmission of PAR is vital because photosynthesis depends on these radiations. Any significant reduction in PAR transmission to the plants

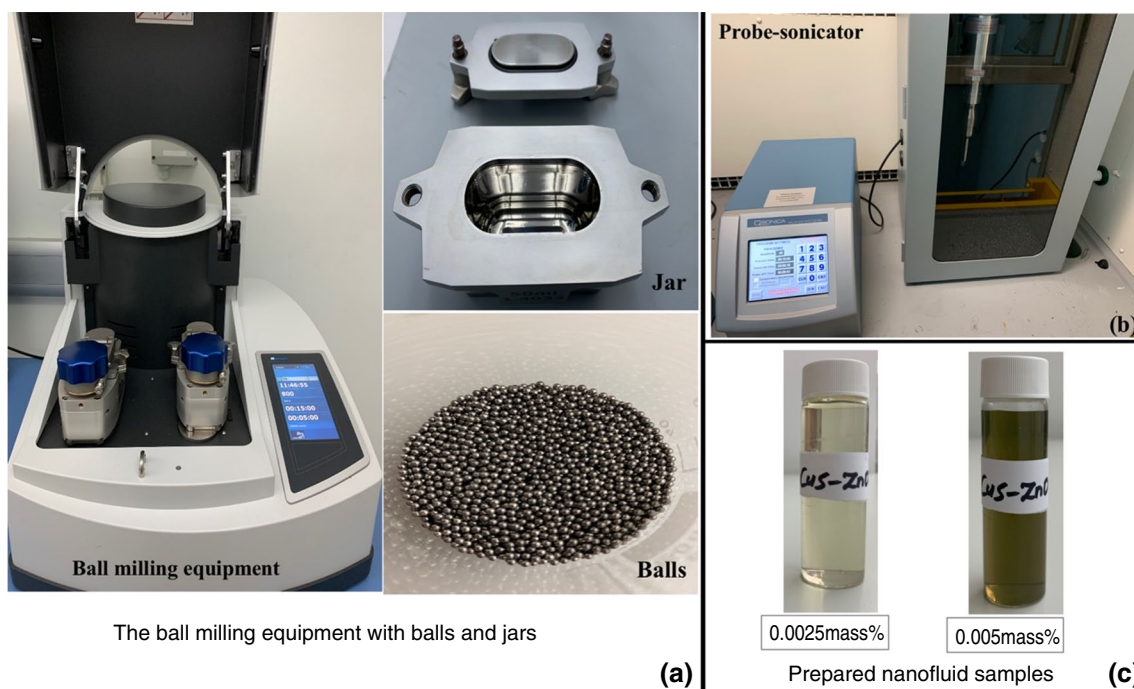


Fig. 2 a Ball milling equipment. b Probe-sonicator. c Prepared nanofluid samples

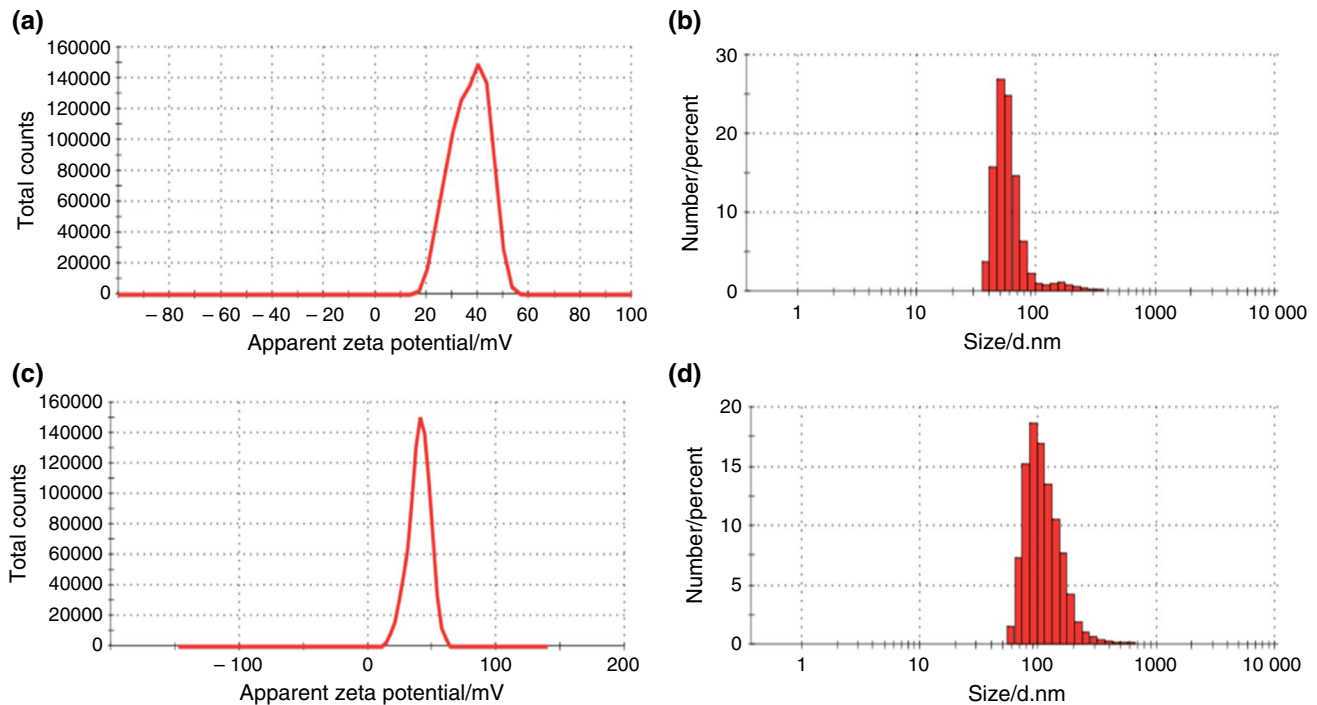


Fig. 3 **a** Zeta potential value for low concentration (0.0025 mass%) nanofluid. **b** Particle size distribution in low concentration (0.0025 mass%) nanofluid. **c** Zeta potential value for high concen-

tration (0.005 mass%) nanofluid. **d** Particles size distribution in high concentration (0.005 mass%) nanofluid

will lead to a decrease in crop yield. Hence, it becomes crucial to investigate the optical transmittance of CuS–ZnO nanofluid. Nanofluids' optical transmittance is evaluated using a UV–VIS–NIR spectrophotometer (UV 3600 plus, SHIMADZU, Japan). The transmittance of nanofluids is assessed using a transparent quartz cuvette with an optical path length of 10 mm. The empty quartz cuvette is kept as a reference in the spectrophotometer during the measurement. Figure 4a depicts the transmittance of water and CuS–ZnO nanofluid (with concentrations of 0.0025 mass% and 0.005 mass%) for an optical path length of 10 mm. The polystyrene sheet is highly transparent in the visible and near-infrared regions. The transparency of polystyrene sheets is nearly similar to water in the visible region. The water can block most radiations having a wavelength greater than 1400 nm (which generally enters the greenhouse and cause higher temperatures).

The transmittance of 0.0025 mass% concentrated nanofluid is higher than 0.005 mass% nanofluid due to less quantity of nanoparticles present in the water. The transmission of 0.005 mass% nanofluid seems very low in the visible region, but it is important to note that this transmission is for an optical path length of 10 mm. This concentration (0.005 mass%) of nanofluid will be used in a 4 mm duct, where the transmission will increase. Figure 4b illustrates the transmittance of 0.0025 mass% and 0.005 mass%

concentrated nanofluids in the respective ducts. The optical transmittance of polystyrene sheet (see Fig. 4 (a)) and ducts containing nanofluids is measured by spectrophotometer (Ocean HDX, from Ocean Insight, USA) in the visible region and (NIR Quest, from Ocean Insight, USA) in the near-infrared region. The average transmittance of duct (4 mm) containing CuS–ZnO nanofluid (0.005 mass%) in the visible region is found to be about 76% (see Fig. 4d). The optical transmission of nanofluid is enhanced with a reduction in optical path length.

The crop growth factor $G(x)$, which represents the ratio of the rate of photosynthesis under greenhouse covering to the rate of photosynthesis under the clear sky, is calculated using [32]:

$$G(x) = \frac{\int_{300}^{800} \tau(x, \lambda) I_0(\lambda) \alpha(\lambda) d\lambda}{\int_{300}^{800} I_0(\lambda) \alpha(\lambda) d\lambda} \quad (1)$$

where $\alpha(\lambda)$ is the relative action spectrum (27 herbaceous plants [33]). Figure 4c shows the relative action spectrum and A.M 1.5 spectral irradiance. It is evident from the graph that the action spectrum contains two peaks: one is near 430 nm, and the other is around 660 nm. The plant organs tend to bend toward or away from a blue light source called a phototropic response. This phototropic response is related to the blue band in the visible spectrum. In comparison, the red

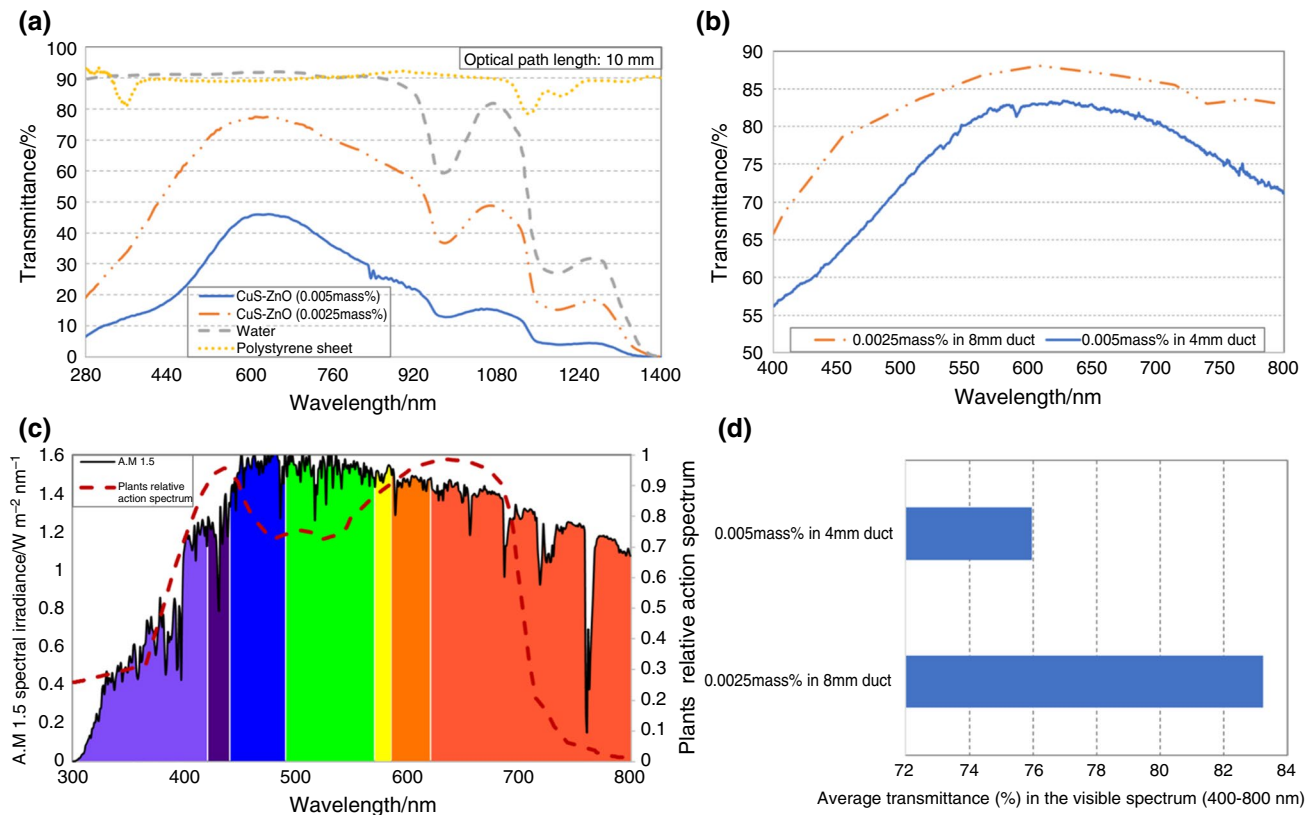


Fig. 4 **a** The transmittance of water, CuS–ZnO nanofluid (0.0025 mass% and 0.005 mass%) for an optical path length of 10 mm. The transmittance of polystyrene sheet used in experimentation. **b** The visible spectrum transmission through specified ducts

having nanofluids **c** A.M 1.5 spectral irradiance and average relative action spectrum of plants. **d** Average transmittance in the visible spectrum for 4 mm and 8 mm duct containing 0.005 mass% and 0.0025 mass% CuS–ZnO nanofluids, respectively

band of visible spectrum is involved in the photosynthesis process [34–36].

Experimental setup and procedure

Two hollow containers (ducts) are prepared from highly transparent polystyrene sheets. The depth (distance between two sheets) of one duct is kept as 4 mm and 8 mm for the other. The silicon rubber (having a width of 3 cm) is used between two sheets as a sealant. These sheets are tightened together through nuts and bolts to prevent leakage, and the duct can bear the pressure of flowing fluid. The duct has an inlet on the bottom side and an outlet at the top (see Fig. 5). To keep the duct wholly filled with fluid (provide no space for air inside the duct) entire time, these positions of inlet and outlet are selected. Two thermocouples (Extech) are installed at the inlet and outlet of duct to measure the temperature of fluid entering and leaving the duct. The prepared duct is attached in front of a small greenhouse unit having dimensions of (45 cm × 22 cm × 35 cm). The walls and roof of the greenhouse unit are made of polystyrene sheets and

supported by a steel frame. Three thermocouples are placed inside this greenhouse unit at various locations (to cover the entire space), and the average of these temperature values is used in the final calculations. The spectrophotometer fiber cables are inserted into the back wall of the greenhouse unit. A PC radiator (Asetek, Denmark) and fan (Mexn, China) are fixed near the side wall to remove the heat accumulated inside the greenhouse unit (in case of active cooling experiments). The cooled water (at 23 °C) flows through the radiator, and fan circulates the air (using power from a DC power supply (3645A, China)), which loses its heat to the cooled water. The temperatures of cooled water entering and leaving the radiator are measured using two thermocouples.

The spaces between polystyrene sheets and the greenhouse unit frame are filled with hot silicon glue for sealing. After the installation of thermocouples, spectrophotometer fiber cable, and cooling unit (radiator and fan), the greenhouse unit is sealed from the top through heat-insulating tape. The entire setup (greenhouse unit and duct) is placed inside a fume hood and in front of a large area solar simulator (Sciencetech, Canada, with spectral match measurement classification: A) to provide artificial solar light (Illuminated

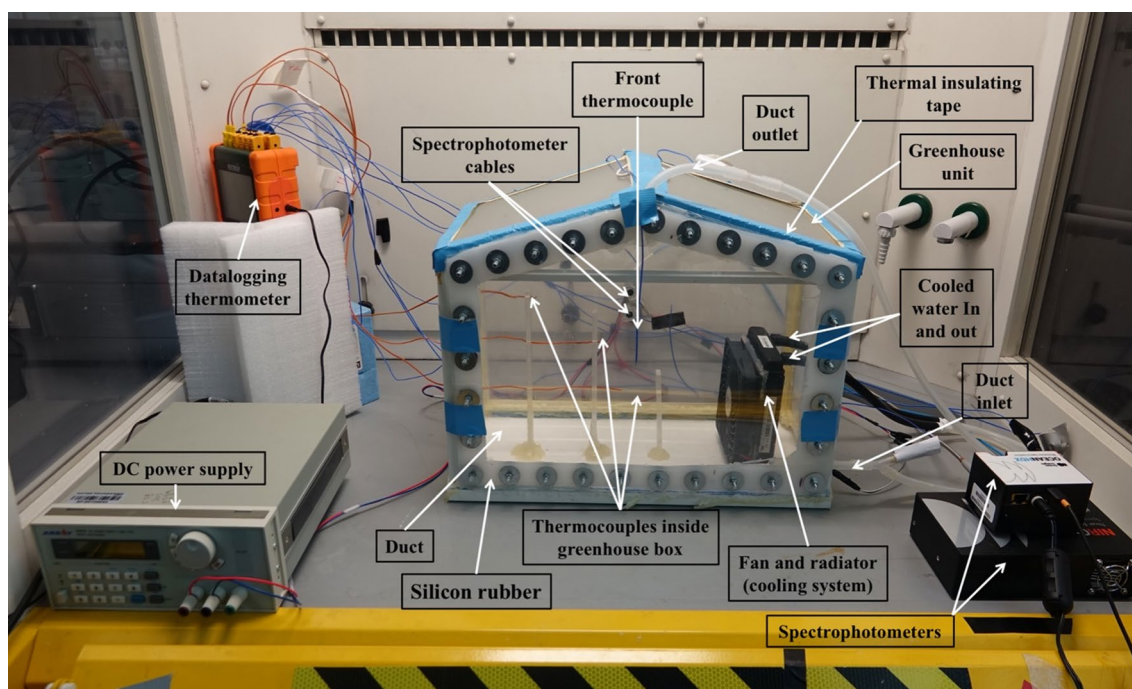


Fig. 5 Experimental setup for greenhouse cooling load reduction using optically tuned nanofluid spectrum filters

area is over $50 \text{ cm} \times 50 \text{ cm}$). The solar simulator can provide solar flux ranging from 500 to 1000 W m^{-2} by varying light intensity from 0.5 Sun to 1 Sun. Greenhouses in hot arid environments have high cooling load issues in summer when ambient temperature and solar irradiance are high. Therefore, an electrical air heater is used to replicate the higher ambient temperature conditions (not in direct contact with the greenhouse). This air heater raised the air temperature inside the fume hood around the greenhouse unit walls. Four thermocouples (on each side of the greenhouse unit) are fixed to measure the ambient temperature inside the fume hood. A 12 channel-data logging thermometer (Extech TM500) is used to measure and record the temperature values at a sampling rate of 2 s .

The fluid (water or nanofluid) is pumped from a storage tank to the duct. The nanofluid flowing through the duct acts as a spectrum filter (transmits specified radiations and absorbs or reflects others). This heated fluid (the temperature of fluid will rise due to absorption of solar radiations) then enters a coil heat exchanger, which is placed inside the refrigerated circulator to dissipate its heat and then pumped back to the storage tank. Note that in real greenhouse applications, underground soil can act as the heat sink to reject this heat. Hence, the nanofluid can be used in a cycle.

To maintain duct shape and ensure smooth flow, two pumps are used at the inlet and outlet of the duct. The pumps are calibrated to measure fluid flow rate after installation in the flow circulation path. To validate the accuracy of pumps,

a highly precise flask is used to measure the flow rate of the fluid. The refrigerated circulator (SD7LR-20-A12E, Polyscience, USA) provides cooled water at a constant temperature of $23 \text{ }^\circ\text{C}$ to the radiator. For the circulation of cooled water from the refrigerated circulator to the radiator, a pump (FlexiPump, France) is used.

Performance assessment

The photothermal conversion efficiency of CuS–ZnO/water nanofluid (having concentrations of 0.0025 mass% and 0.005 mass%) is calculated by using Eq. (2).

$$\eta_{\text{th}} = \frac{\dot{m}_{\text{nf}} C_{\text{p,nf}} (T_{\text{out}} - T_{\text{in}})}{IA_{\text{duct}}} \quad (2)$$

The specific heat of nanofluid $C_{\text{p,nf}}$ can be estimated as given by [37]:

$$C_{\text{p,nf}} = \frac{\varnothing \rho_{\text{np}} C_{\text{p,np}} + (1 - \varnothing) \rho_{\text{bf}} C_{\text{p,bf}}}{\rho_{\text{nf}}} \quad (3)$$

The volume fraction (\varnothing) and density of nanofluid (ρ_{nf}) can be calculated as:

$$\varnothing = \left(\frac{\frac{m_{\text{np}}}{\rho_{\text{np}}}}{\frac{m_{\text{np}}}{\rho_{\text{np}}} + \frac{m_{\text{bf}}}{\rho_{\text{bf}}}} \right) \quad (4)$$

Table 1 Measuring instruments accuracies

Instrument	Thermocouple	Datalogger	Pump (flow rate)	Spectrophotometer
Accuracy	$\pm 0.1\text{ }^{\circ}\text{C}$	$\pm 0.1\text{ }^{\circ}\text{C}$	$\pm 0.1\text{ Lh}^{-1}$	$\pm 0.2\text{ nm}$ in the UV–VIS region $\pm 0.8\text{ nm}$ in the NIR region

$$\rho_{\text{nf}} = \emptyset \rho_{\text{np}} + (1 - \emptyset) \rho_{\text{bf}} \quad (5)$$

The total heat gained by cooled water (from the radiator) is given by Eq. (6).

$$\dot{Q}_{\text{cooling}} = \int_0^t (\dot{m}_{\text{water}} C_{p,\text{water}} \Delta T) dt \quad (6)$$

where ΔT is the difference in the temperature of cooled water leaving the radiator and entering the radiator.

Uncertainty analysis

There are some uncertainties associated with experimental results. In the present study, Kline and McClintock's [38] method is used to estimate the uncertainties. The best estimate for a variable can be given as

$$z = z_{\text{measured}} \pm \delta z \quad (7)$$

So, the final result should lie within $\pm \delta z$ of the actual value. The final result, z_R , could be a function of several measured quantities, and each quantity will have a different uncertainty value.

$$z_R = f(z_1, z_2, z_3, \dots, z_n) \quad (8)$$

The expression suggested by Kline and McClintock [38] to estimate the resulting uncertainty, δz_R in the dependent variable z_R is given as

$$\delta z_R = \left[\left(\frac{\partial f}{\partial z_1} \delta z_1 \right)^2 + \left(\frac{\partial f}{\partial z_2} \delta z_2 \right)^2 + \left(\frac{\partial f}{\partial z_3} \delta z_3 \right)^2 + \dots + \left(\frac{\partial f}{\partial z_n} \delta z_n \right)^2 \right]^{1/2} \quad (9)$$

The accuracies of measuring equipment are given in Table 1. The maximum uncertainties associated with heat gained and photothermal conversion efficiency were 1.35% and 1.42%, respectively.

Results and discussion

Solar irradiance is abundantly available in many countries throughout the year. The hourly global horizontal irradiation (GHI) received by one of such a country (e.g., Qatar) is found from SMARTS software, developed by NREL [39]. The data showed that the global horizontal irradiance is more than 500 W m^{-2} for nearly 9 h in summer and 5 h in winter. The peaks of this solar irradiance reached near 1000 W m^{-2} in summer and 650 W m^{-2} in winter (in such

countries, winter has a short period while summer covers a significant portion of the year). The minimum irradiance used in the present experimental work is 500 W m^{-2} . The irradiance value is increased by 100 W m^{-2} after 15 min (900 s) until it reaches a maximum value of 1000 W m^{-2} , thus making the total duration of a single experiment up to 5400 s. To simplify the results, the ambient temperature is classified into two categories (Low and High). The low ambient temperature has a range between 22 to $28\text{ }^{\circ}\text{C}$. While the high ambient temperature has a range between 32 to $38\text{ }^{\circ}\text{C}$. The cooled water (at $23\text{ }^{\circ}\text{C}$) circulates in the radiator, and a fan circulates the air inside the greenhouse unit. The high-temperature air loses its heat to the cooled water. Initially, the heat gained by the cooling system was found at various flow rates. The heat gain by cooling system becomes nearly constant after a specific coolant flow rate. This flow rate of coolant is used in experiments. The coolant flow rates at low and high ambient temperature conditions are selected as 6.4 mL s^{-1} and 7.6 mL s^{-1} , respectively.

Figure 6 depicts the inside temperature of greenhouse unit when the cooling system is off, and ambient temperature is low. The inside temperature of greenhouse unit is higher when the ducts are empty (no fluid is flowing through the ducts). The greenhouse unit temperature kept rising due to the heat accumulation from solar radiation. For empty duct case, the inside temperature of greenhouse unit is same ($43.2\text{ }^{\circ}\text{C}$) for 8 mm and 4 mm ducts at the end of experiment. The air inside the duct does not provide any hindrance to radiation, due to which the greenhouse unit inside temperature is identical irrespective of duct thickness. When water flows through the ducts, the greenhouse unit with 8 mm duct displayed ($2.43\text{ }^{\circ}\text{C}$) lower inside temperature than the greenhouse unit with 4 mm duct. The water has potential to absorb some infrared radiations. This absorption is highly dependent on the optical path length. The 8 mm duct provides more optical path length than 4 mm duct, due to which water can absorb more radiations. That is why the greenhouse unit attained a lower rise in temperature when 8 mm duct was attached compared to 4 mm duct. The inside temperature of greenhouse unit is $36.6\text{ }^{\circ}\text{C}$ and $36.8\text{ }^{\circ}\text{C}$ for 8 mm and 4 mm ducts, respectively, when CuS–ZnO nanofluid flows through the ducts. The 8 mm duct contained a lower concentrated nanofluid. In comparison, the 4 mm duct had a higher concentrated nanofluid, due to which the inside temperature of greenhouse unit is nearly identical for two cases.

Figure 7 illustrates the inside temperature of greenhouse unit when the cooling system is on, and ambient temperature

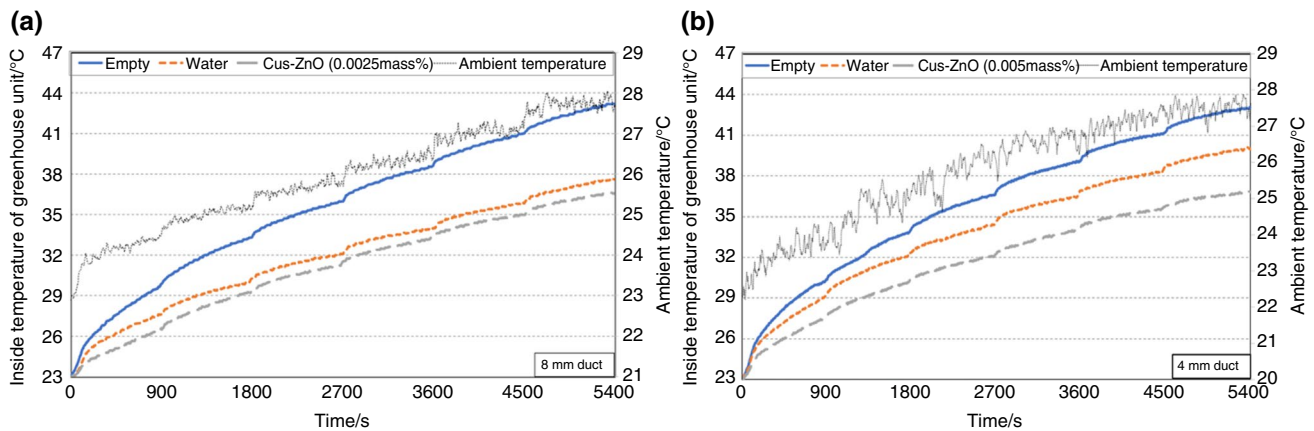


Fig. 6 Inside temperature of greenhouse unit – cooling system is OFF and ambient temperature is LOW **a** 8 mm duct **b** 4 mm duct

is low. The cooling system restricted the inside temperature of greenhouse unit to 28 °C for empty ducts. When water flows through ducts, the 8 mm duct caused a 0.4 °C reduction in the inside temperature of greenhouse unit than the 4 mm duct case. In the case of nanofluid, the temperature of greenhouse unit remained nearly identical for both ducts.

Figure 8 represents the inside temperature of greenhouse unit when the cooling system is on, and the ambient temperature is high. The significant portion of greenhouse cooling load is due to solar irradiance and heat entering through the greenhouse covers. At higher ambient temperature, the heat entering through the covers increases and cause a rise in the cooling load. Due to aforementioned reason, the inside temperature of greenhouse unit will rise with an increase in ambient temperature. For empty duct cases, the inside temperature of greenhouse unit is 1.6 °C higher for high ambient temperature case than the low ambient temperature case. The 8 mm duct showed 0.3 °C less temperature inside the greenhouse unit than the 4 mm duct when water flowed through

the ducts. For the case of nanofluid, the greenhouse unit inside temperature is 0.4 °C higher for 4 mm duct than the 8 mm duct. The possible reason for this higher greenhouse unit temperature is a lower optical path length of 4 mm duct than 8 mm duct.

Figure 9 shows the % reduction in heat gained by cooling system compared to respective empty ducts for low and high ambient temperatures. The % reduction in heat gain is higher when nanofluid flowed through the ducts than the water under all ambient temperature conditions. This is due to optically tuned characteristics of CuS–ZnO nanofluid, which has potential to block more portion of the infrared region than water. The % reduction in heat gain is higher for 8 mm duct than the 4 mm duct. From this result, it can be inferred that the optical path length played a major role in reducing the transmittance of infrared radiations inside the greenhouse unit than the concentration of nanoparticles. The average % reduction in heat gain compared to an empty duct (8 mm) for CuS–ZnO nanofluid is 27.4%. The % reduction

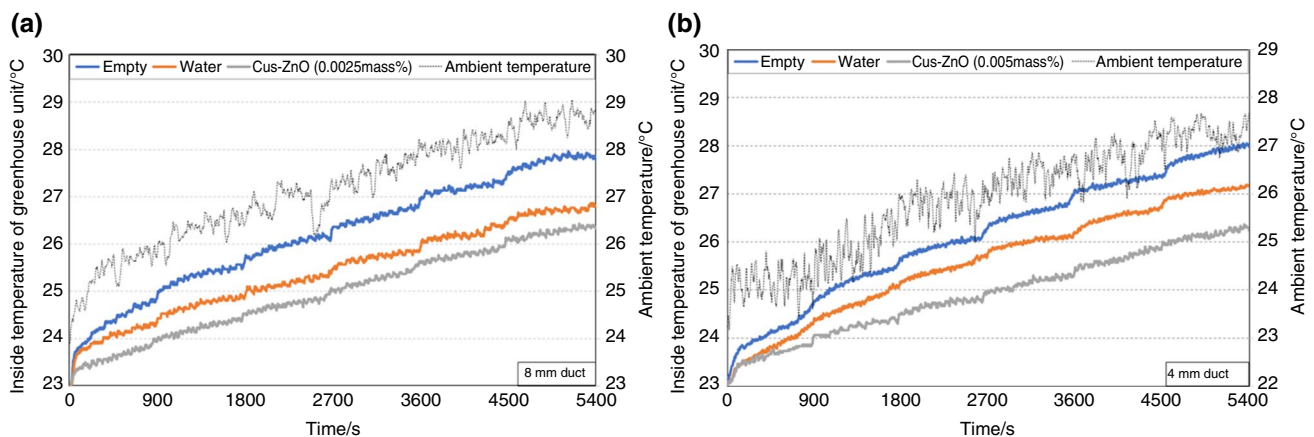


Fig. 7 Inside temperature of greenhouse unit – cooling system is ON, and ambient temperature is LOW **a** 8 mm duct **b** 4 mm duct

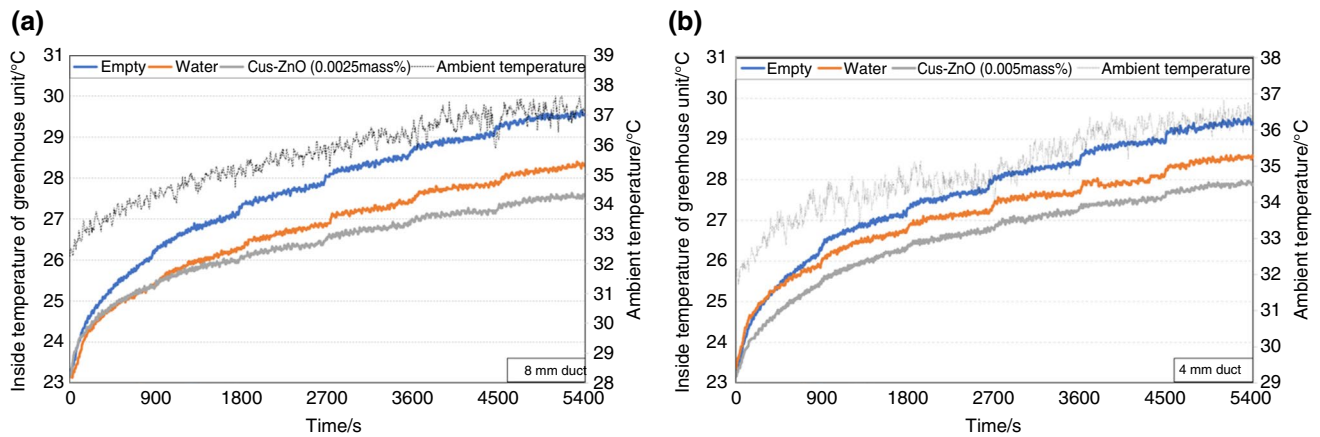


Fig. 8 Inside temperature of greenhouse unit – cooling system is ON, and ambient temperature is HIGH **a** 8 mm duct **b** 4 mm duct

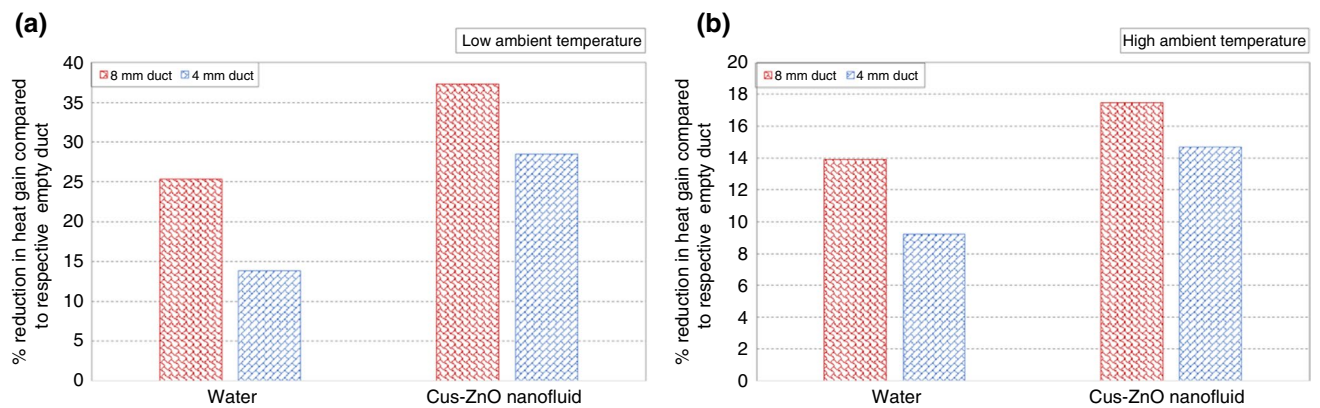


Fig. 9 % reduction in heat gain by cooling system for the cases when fluid (water or nanofluid) is flowing in the duct compared to the case when no fluid is flowing through the respective duct: **a** Low ambient temperature. **b** High ambient temperature

in heat gain by cooling system deteriorates with the rise in ambient temperature due to an increase in heat entering through the covers.

Figure 10 (a) and (b) exhibits the difference in outlet and inlet temperature of water and nanofluid flowing through the ducts. The water and CuS–ZnO nanofluid flowing through the duct is exposed to 1 Sun for 20 min at a flow rate of 340 mL s^{-1} . The difference in outlet and inlet temperature of fluid flowing through 8 mm duct is higher than the 4 mm duct. The longer optical path length allowed water or nanofluid to absorb more radiation, resulting in higher outlet temperature compared to a lower optical path length. For the case of nanofluid, the 4 mm duct showed a rapid increase in temperature at the start due to a higher concentration of nanoparticles. The higher quantity of nanoparticles strengthens the Brownian motion inside the fluid. That is why the temperature rise at the start for 4 mm duct is higher than 8 mm duct. The 8 mm duct achieved a higher temperature difference than the 4 mm duct after 500 s. Figure 10c and d

depicts the photothermal conversion efficiency for both ducts containing water and nanofluid, respectively. The 8 mm duct showed better photothermal conversion efficiency than the 4 mm duct in each case. The 8 mm duct displayed a nearly 25% higher photothermal conversion efficiency than 4 mm for water, which improved to 26.32% for the nanofluid case. This is due to the thicker fluid layer, which has a larger optical path length and can absorb more radiation.

The photosynthetic photon flux density (PPFD) represents the number of photons in a specific wavelength range (400–700 nm) being incident on a surface per unit time and per unit surface area. If the amount of PPFD incidents on a crop is less than the required amount, the crop yield may decrease. The ranges of PPFD required by various plants are found in the literature and summarized in Table 2. Figure 11a and b represents the PPFD obtained inside the greenhouse unit at 0.5 and 1 sun, respectively. The PPFD was higher inside the greenhouse unit when the ducts were empty. Although there is a slight reduction in

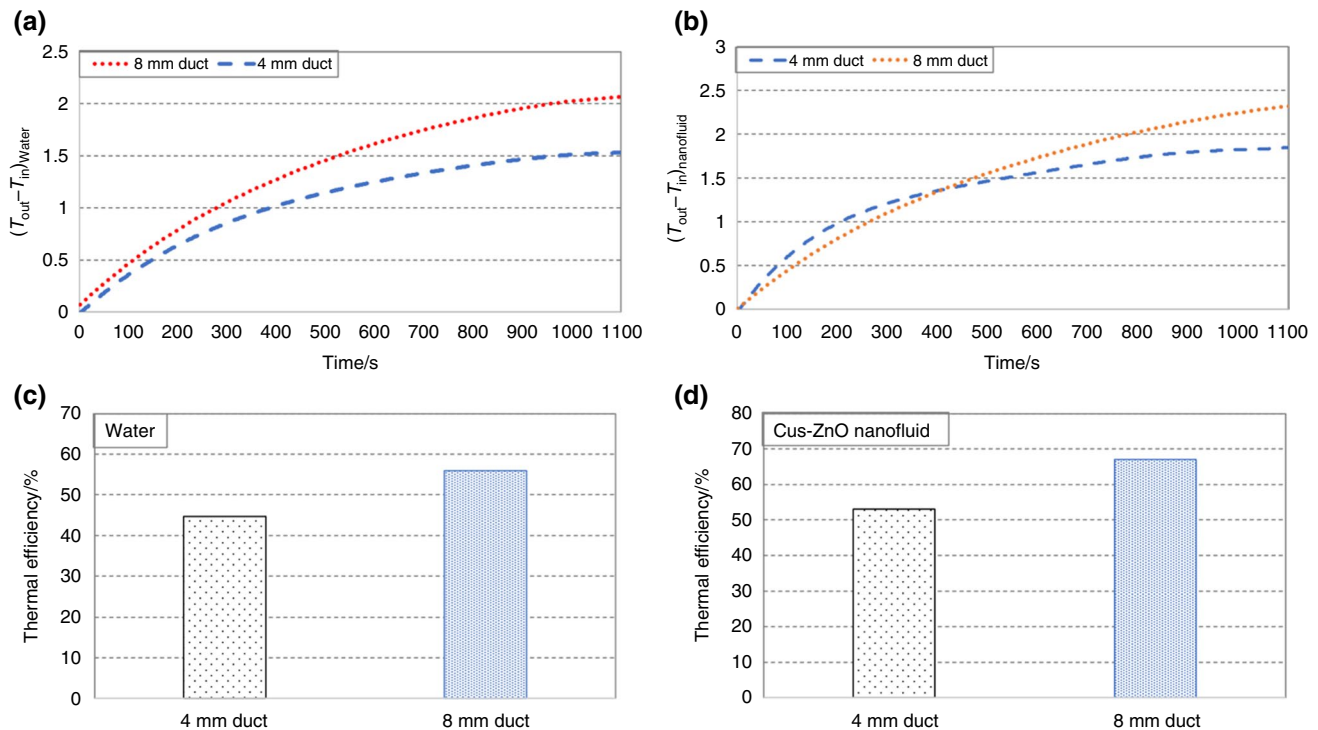


Fig. 10 Difference in outlet and inlet temperature of **a** water and **b** CuS–ZnO nanofluid flowing through the duct. The photothermal conversion efficiency of **c** water and **d** CuS–ZnO nanofluid flowing through the duct

PPFD by application of nanofluid, the results revealed that using nanofluid could provide more PPFD than the essential requirement of many plants. This means the application of nanofluid will have an insignificant impact on crop yield.

Figure 11c shows the crop growth factor calculated for 4 mm and 8 mm ducts. It is evident from the graph that the crop growth factor is higher for 8 mm duct. The increase in nanoparticle concentration blocked the photosynthetically active radiations more, which resulted in a reduction of crop growth factor for the 4 mm duct case. Figure 11d exhibits the crop growth factor value for the present study (8 mm duct) and the values available in literature. The crop growth factor is significantly lower when semi-transparent organic

solar cells [1, 6] are used as spectrum filters than spectrum-selective nanofluids.

Payback period of nanofluid system

The application of spectrum-selective (CuS–ZnO) nanofluid exhibited a reduction in heat gained by the cooling system compared to reference case (empty duct). This heat gain reduction can reduce the cooling system's size, and thus, the energy required. The payback period (P_{BP}) for 4 mm and 8 mm ducts containing nanofluids is calculated using Eq. (10). The life period (L_p) of system is considered ten years because the cover sheet warranty period is considered for ten years.

Table 2 Ranges of PPFD requirements by various plants

Plant	PPFD / $\mu\text{mol m}^{-2} \text{s}^{-1}$	Plant	PPFD / $\mu\text{mol m}^{-2} \text{s}^{-1}$
African violet	150–250 [40]	Lettuce	250–450 [40]
Beans	336–420 [41]	Lily	250–450 [40]
Carnation	250–450 [40]	Ornamental leaf plants	150–250 [40]
Chrysanthemum	250–450 [40]	Peas	672 [42]
Cucumber	250–450 [40]	Peppers	504 [41, 42]
Eggplant	504 [41, 42]	Poinsettia	250–450 [40]
Geranium	250–450 [40]	Rose	450–750 [40]
Strawberry	250–450 [40]	Tomato	450–750 [40]

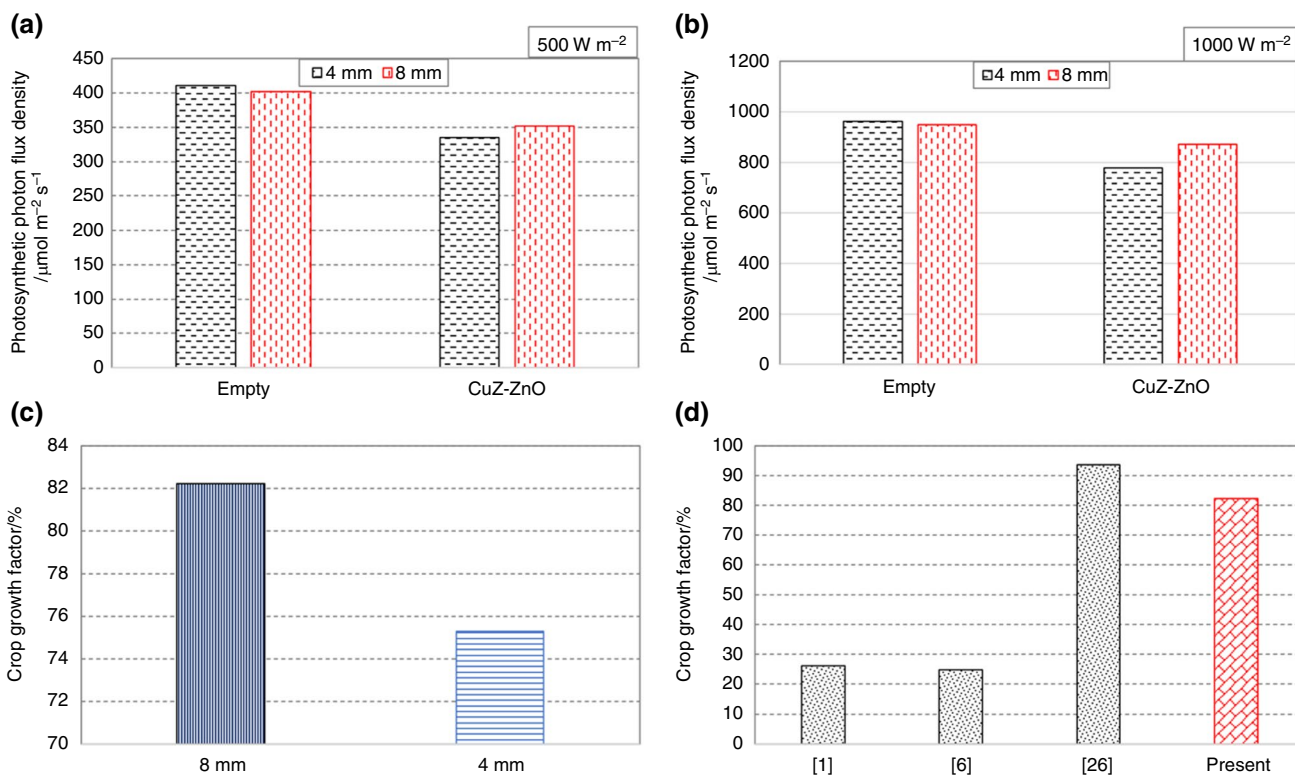


Fig. 11 **a** Photosynthetic photon density (PPFD) obtained inside the greenhouse at 0.5 Sun. **b** Photosynthetic photon density (PPFD) obtained inside the greenhouse at 1 sun. **c** Crop growth factor calculated for CuS–ZnO nanofluid flowing in 4 mm and 8 mm ducts. **d**

Crop growth factor values in the literature for greenhouses that used solar cells ([1, 6]) for spectrum filtering and greenhouses used nanofluid ([26]) for spectrum splitting

$$P_{BP} = \ln\left(1 - \frac{C_C(i_R - f_R)}{C_{SE}}\right) / \ln\left(\frac{1+f_R}{1+i_R}\right) \tag{10}$$

Here, C_{SE} is calculated as

$$C_{SE} = C_E E_S - \left(\frac{C_C(1+i_R)^{L_p}}{(1+i_R)^{L_p} - 1} + C_{O\&M} \right) \tag{11}$$

The annual electricity consumption of a conventional greenhouse for cooling purposes is estimated in the study [9] as 18.1 MWh year⁻¹. Using the results of present experimental work, the annual electricity saving can be calculated as 206 kWh m⁻² for 8 mm duct case and 163 kWh m⁻² for 4 mm duct case (here, m⁻² represents the floor area of a greenhouse). The transmittance of nanofluid will increase with its continuous usage over time. Therefore, the replacement of nanofluid is considered after twelve months during the payback period analysis. The values of various parameters used during the analysis are presented in Table 3.

Figure 12 exhibits the payback period of nanofluid system as a function of the cost of electricity. It can be observed from the graph that the nanofluid system with 8 mm duct

has a lower payback period than the 4 mm duct case. The 8 mm duct showed more reduction in heat gain than 4 mm duct, due to which the payback period is lower for this duct. If the cost of electricity is considered as 0.1 \$ kWh⁻¹, then the payback period for 8 mm and 4 mm ducts becomes 0.42 and 0.55 years, respectively.

Table 3 Values of various parameters used in the economic analysis

Parameter	Value
Interest rate	3.25%
Inflation rate	2.3%
Lifetime	10 years
Cost of nanofluid (for both 4 mm and 8 mm duct) per m ² of duct area	3.3 \$ m ⁻²
Cost of the nanofluid system (Pump and duct in which nanofluid flows)	4.88 \$ m ⁻²
Annual operation and maintenance cost	10% of capital cost
Cost of electricity	0.1 \$ kWh ⁻¹

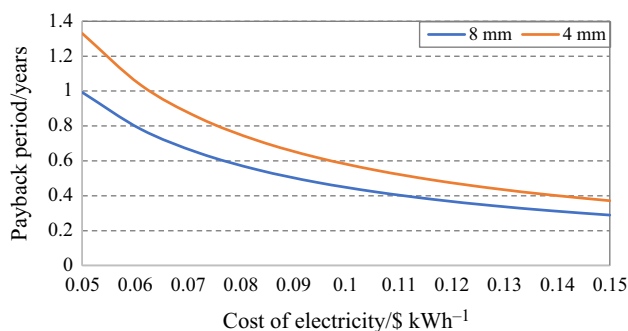


Fig. 12 Payback period of the nanofluid system for 4 mm and 8 mm ducts as a function of the cost of electricity

Conclusions

The present experimental work evaluates the outcomes of application of spectrum-selective CuS–ZnO/water nanofluid on the temperature and heat gained by cooling system of an agricultural greenhouse. The optically tuned CuS–ZnO nanofluid has high transmittance in the visible region of solar spectrum with good near-infrared blocking capability. The spectrum-selective CuS–ZnO/water nanofluids were synthesized (0.0025 mass% and 0.005 mass%), and stability, particle size distribution, and optical transmission of prepared nanofluids were examined. The prepared concentrations of nanofluids were used in the experimental setup (4 mm and 8 mm ducts). The following conclusions can be drawn based on obtained results:

- Both concentrations of CuS–ZnO/water nanofluid exhibited good dispersion and stability in the base fluid. The average transmittance in visible spectrum for 0.005 mass% concentrated nanofluid was 76% in 4 mm duct, while for 0.0025 mass% concentration, this transmittance enhanced to 83% in the 8 mm duct.
- The indoor temperature of the greenhouse unit remained nearly the same for empty ducts, irrespective of duct thickness. For the case when water flowed through the ducts, the 8 mm duct performed much better than the 4 mm duct due to the larger optical path length. Under all tested ambient temperature conditions, the inside temperature of greenhouse unit was lower (about an average of 3.4 °C) when nanofluid was flowing through the ducts than the empty duct.
- The cooling system gained less heat when water or nanofluid flowed through the ducts. The % reduction in heat gain by the cooling system compared to the empty duct was higher for 8 mm duct case than 4 mm duct. The cooling system showed an average 27.4% and 21.6% reduction in heat gain for 8 mm and 4 mm ducts, respectively, when nanofluid was flowing.

- The 8 mm duct showed a higher difference in temperature at the outlet and inlet for water and nanofluid than the 4 mm duct. Adding a small quantity of nanoparticles improves the photothermal conversion efficiency of water.
- The crop growth factor values calculated for 4 mm and 8 mm duct cases are 75.3% and 82.2%, respectively. The photosynthetic photon flux density inside the greenhouse unit was higher than many plants' requirements, indicating that the plant's growth will not be affected by applying spectrum-selective nanofluids.
- The payback period was strongly dependent on the cost of electricity. For electricity cost of 0.1 \$ kWh⁻¹, the payback period for 4 mm and 8 mm ducts was estimated to be 0.55 and 0.42 years, respectively.

In future, more experimental research is required to find other nanomaterials with better optical characteristics and long-term exposure to sunlight for greenhouse applications. Such nanomaterials will help further reduction in agricultural greenhouses' cooling load in hot arid climates.

Acknowledgements Open Access funding provided by the Qatar National Library. The authors acknowledge the support provided by the Hamad Bin Khalifa University, Qatar Foundation, Qatar (210024930). This publication was made possible by NPRP grant NPRP12S-0123-190011 from the Qatar National Research Fund (a member of Qatar Foundation).

Funding Open Access funding provided by the Qatar National Library.

Declarations

Conflict of interest The authors (M.U.S. and Y.B.) declare that they have a pending patent "Greenhouse and cooling system of the same," US20220007592A1.

Open Access This article is licensed under a Creative Commons Attribution 4.0 International License, which permits use, sharing, adaptation, distribution and reproduction in any medium or format, as long as you give appropriate credit to the original author(s) and the source, provide a link to the Creative Commons licence, and indicate if changes were made. The images or other third party material in this article are included in the article's Creative Commons licence, unless indicated otherwise in a credit line to the material. If material is not included in the article's Creative Commons licence and your intended use is not permitted by statutory regulation or exceeds the permitted use, you will need to obtain permission directly from the copyright holder. To view a copy of this licence, visit <http://creativecommons.org/licenses/by/4.0/>.

References

1. Wang D, Liu H, Li Y, Zhou G, Zhan L, Zhu H, et al. High-performance and eco-friendly semitransparent organic solar cells for greenhouse applications. *Joule*. 2021;5:945–57.
2. Ravishankar E, Charles M, Xiong Y, Henry R, Swift J, Rech J, et al. Balancing crop production and energy harvesting in organic solar-powered greenhouses. *Cell Reports Phys Sci*. 2021;2

3. Duan L, Hoex B, Uddin A. Progress in semitransparent organic solar cells. *Sol RRL*. 2021;5.
4. Xu T, Luo Y, Wu S, Deng B, Chen S, Zhong Y, et al. High-performance semitransparent organic solar cells: from competing indexes of transparency and efficiency perspectives. *Adv Sci*. 2022;2202150.
5. Song W, Fanady B, Peng R, Hong L, Wu L, Zhang W, et al. Foldable semitransparent organic solar cells for photovoltaic and photosynthesis. *Adv Energy Mater*. 2020;10.
6. Shi H, Xia R, Zhang G, Yip HL, Cao Y. Spectral engineering of semitransparent polymer solar cells for greenhouse applications. *Adv Energy Mater*. 2019;9.
7. Hu Z, Wang Z, An Q, Zhang F. Semitransparent polymer solar cells with 12.37% efficiency and 18.6% average visible transmittance. *Sci Bull*. 2020;65:131–7.
8. Loik ME, Carter SA, Alers G, Wade CE, Shugar D, Corrado C, et al. Wavelength-selective solar photovoltaic systems: powering greenhouses for plant growth at the food-energy-water nexus. *Earth's Futur*. 2017;5:1044–53.
9. Bicer Y, Sajid MU, Al-Breiki M. Optimal spectra management for self-power producing greenhouses for hot arid climates. *Renew Sustain Energy Rev*. 2022;159.
10. Chavan SG, Maier C, Alagoz Y, Filipe JC, Warren CR, Lin H, et al. Light-limited photosynthesis under energy-saving film decreases eggplant yield. *Food Energy Secur*. 2020;9.
11. Pakari A, Ghani S. Evaluation of a novel greenhouse design for reduced cooling loads during the hot season in subtropical regions. *Sol Energy*. 2019;181:234–42.
12. Sonneveld PJ, Swinkels GLAM, Bot GPA, Flamand G. Feasibility study for combining cooling and high grade energy production in a solar greenhouse. *Biosyst Eng*. 2010;105:51–8.
13. Alinejad T, Yaghoubi M, Vadiiee A. Thermo-environmental assessment of an integrated greenhouse with an adjustable solar photovoltaic blind system. *Renew Energy*. 2020;156:1–13.
14. Basit Shafiq M, Allauddin U, Qaisrani MA, Rehman ur T, Ahmed N, Usman Mushtaq M, et al. Thermal performance enhancement of shell and helical coil heat exchanger using MWCNTs/water nanofluid. *J Therm Anal Calorim*. 2022;147:12111–26.
15. Sajid MU, Ali HM, Bicer Y. Exergetic performance assessment of magnesium oxide–water nanofluid in corrugated minichannel heat sinks: An experimental study. *Int J Energy Res*. 2022;46:9985–10001.
16. Khan A, Ali HM, Nazir R, Ali R, Munir A, Ahmad B, et al. Experimental investigation of enhanced heat transfer of a car radiator using ZnO nanoparticles in H₂O–ethylene glycol mixture. *J Therm Anal Calorim*. 2019;138:3007–21.
17. Sajid MU, Bicer Y. Impacts of ultrasonication time and surfactants on stability and optical properties of CuO, Fe₃O₄, and CNTs/water nanofluids for spectrum selective applications. *Ultrason Sonochem*. 2022;88: 106079.
18. Sajid MU, Bicer Y. Nanofluids as solar spectrum splitters: a critical review. *Sol Energy*. 2020;207:974–1001.
19. Huang J, Han X, Zhao X, Khosa AA, Meng C. The stability, optical behavior optimization of Ag@SiO₂ nanofluids and their application in spectral splitting photovoltaic/thermal receivers. *Renew Energy*. 2022;190:865–78.
20. Li H, He Y, Wang C, Wang X, Hu Y. Tunable thermal and electricity generation enabled by spectrally selective absorption nanoparticles for photovoltaic/thermal applications. *Appl Energy*. 2019;236:117–26.
21. Ekiciler R, Arslan K, Turgut O, Kurşun B. Effect of hybrid nanofluid on heat transfer performance of parabolic trough solar collector receiver. *J Therm Anal Calorim*. 2021;143:1637–54.
22. Mahbubul IM, Khan MMA, Ibrahim NI, Ali HM, Al-Sulaiman FA, Saidur R. Carbon nanotube nanofluid in enhancing the efficiency of evacuated tube solar collector. *Renew Energy*. 2018;121:36–44.
23. Akram N, Sadri R, Kazi SN, Zubir MNM, Ridha M, Ahmed W, et al. A comprehensive review on nanofluid operated solar flat plate collectors. *J Therm Anal Calorim*. 2020;139:1309–43.
24. Wahab A, Hassan A, Qasim MA, Ali HM, Babar H, Sajid MU. Solar energy systems – Potential of nanofluids. *J Mol Liq*. 2019;289.
25. Loni R, Asli-Ardeh EA, Ghobadian B, Kasaeian A. Experimental study of carbon nano tube/oil nanofluid in dish concentrator using a cylindrical cavity receiver: outdoor tests. *Energy Convers Manag*. 2018;165:593–601.
26. Yuan Y, Fang H, Wu G, Yang Q, Ma Q, Ji Y, et al. Experimental investigation of full solar spectrum utilization based on nanofluid spectral splitter for greenhouse applications. *Energy Convers Manag*. 2022;254.
27. Liu X, Shen C, Wang J. Investigation on the lighting/heating performance of tubular daylighting devices (TDDs) based on nanofluids. *Energy Build*. 2022;263.
28. Sajid MU, Bicer Y. Performance Assessment of Spectrum Selective Nanofluid-Based Cooling for a Self-Sustaining Greenhouse. *Energy Technol*. 2021;9:2000875.
29. Marcelis LFM, Broekhuijsen AGM, Meinen E, Nijs EMFM, Raaphorst MGM. Quantification of the growth response to light quantity of greenhouse grown crops. *Acta Hortic*. 2006;711:97–103.
30. Shah J, Ranjan M, Thareja P, Estellé P. Tailoring stability and thermophysical properties of CuO nanofluid through ultrasonication. *J Therm Anal Calorim*. 2022;147:10319–28.
31. Kanti P, Sharma K V., Khedkar RS, Rehman T ur. Synthesis, characterization, stability, and thermal properties of graphene oxide based hybrid nanofluids for thermal applications: Experimental approach. *Diam Relat Mater*. 2022;128.
32. La Notte L, Giordano L, Calabrò E, Bedini R, Colla G, Puglisi G, et al. Hybrid and organic photovoltaics for greenhouse applications. *Appl Energy*. 2020;278.
33. Katsumi I. Action spectra for photosynthesis in higher plants. *Plant Cell Physiol*. 1976;17.
34. Smith H. Phytochromes and light signal perception by plants - An emerging synthesis. *Nature*. 2000;407:585–91.
35. Gilberto L, Perrotta G, Pallara P, Weller JL, Fraser PD, Bramley PM, et al. Manipulation of the blue light photoreceptor cryptochrome 2 in tomato affects vegetative development, flowering time, and fruit antioxidant content. *Plant Physiol*. 2005;137:199–208.
36. Viczián A, Klose C, Ádám É, Nagy F. New insights of red light-induced development. *Plant Cell Environ*. 2017;40:2457–68.
37. Yimin X, Wilfried R. Conceptions for heat transfer correlation of nanofluids. *Int J Heat Mass Transf*. 2000;43:3701–7.
38. Kline SJ. Describing uncertainty in single sample experiments. *Mech Eng*. 1954;75(3–8):1–9.
39. Gueymard CA. SMARTS2: a simple model of the atmospheric radiative transfer of sunshine: algorithms and performance assessment. Rep No FSEC-PF-270–95 [Internet]. 1995;1–84. Available from: <http://institutesre.org/GCCE/SMARTS2.pdf>
40. Albright, L.D. *Plant Growth Chamber Handbook*; Iowa Agriculture and Home Economics Experiment Station Special Report No. 99; Cornell University: Ithaca, NY, USA, 1998.
41. Somerville C, Cohen M, Pantanella E, Stankus A, Lovatelli A. Small-scale aquaponic food production. *Integrated fish and plant farming*. FAO Fish Aquac. 2014;262.
42. Tazawa S. Effects of various radiant sources on plant growth (Part 1). *Japan Agric Res Q*. 1999;33:163–76.

Publisher's Note Springer Nature remains neutral with regard to jurisdictional claims in published maps and institutional affiliations.